Monthly Notices of the ROYAL ASTRONOMICAL SOCIETY
MNRAS **444,** 776–789 (2014) doi:10.1093/mnras/stu1492

High-precision photometry by telescope defocussing – VI. WASP-24, WASP-25 and WASP-26★

John Southworth,[1]† T. C. Hinse,[2] M. Burgdorf,[3] S. Calchi Novati,[4,5] M. Dominik,[6]‡ P. Galianni,[6] T. Gerner,[7] E. Giannini,[7] S.-H. Gu,[8,9] M. Hundertmark,[6] U. G. Jørgensen,[10] D. Juncher,[10] E. Kerins,[11] L. Mancini,[12] M. Rabus,[13,12] D. Ricci,[14] S. Schäfer,[15] J. Skottfelt,[10] J. Tregloan-Reed,[1,16] X.-B. Wang,[8,9] O. Wertz,[17] K. A. Alsubai,[18] J. M. Andersen,[10,19] V. Bozza,[4,20] D. M. Bramich,[18] P. Browne,[6] S. Ciceri,[12] G. D'Ago,[4,20] Y. Damerdji,[17] C. Diehl,[7,21] P. Dodds,[6] A. Elyiv,[22,17,23] X.-S. Fang,[8,9] F. Finet,[17,24] R. Figuera Jaimes,[6,25] S. Hardis,[10] K. Harpsøe,[10] J. Jessen-Hansen,[26] N. Kains,[27] H. Kjeldsen,[26] H. Korhonen,[28,10] C. Liebig,[6] M. N. Lund,[26] M. Lundkvist,[26] M. Mathiasen,[10] M. T. Penny,[29] A. Popovas,[10] S. Prof.,[7] S. Rahvar,[30] K. Sahu,[27] G. Scarpetta,[5,4,20] R. W. Schmidt,[7] F. Schönebeck,[7] C. Snodgrass,[31] R. A. Street,[32] J. Surdej,[17] Y. Tsapras[32,33] and C. Vilela[1]

Affiliations are listed at the end of the paper

Accepted 2014 July 23. Received 2014 July 22; in original form 2014 May 28

ABSTRACT

We present time series photometric observations of 13 transits in the planetary systems WASP-24, WASP-25 and WASP-26. All three systems have orbital obliquity measurements, WASP-24 and WASP-26 have been observed with *Spitzer*, and WASP-25 was previously comparatively neglected. Our light curves were obtained using the telescope-defocussing method and have scatters of 0.5–1.2 mmag relative to their best-fitting geometric models. We use these data to measure the physical properties and orbital ephemerides of the systems to high precision, finding that our improved measurements are in good agreement with previous studies. High-resolution *Lucky Imaging* observations of all three targets show no evidence for faint stars close enough to contaminate our photometry. We confirm the eclipsing nature of the star closest to WASP-24 and present the detection of a detached eclipsing binary within 4.25 arcmin of WASP-26.

Key words: stars: fundamental parameters – planetary systems – stars: individual: WASP-24 – stars: individual: WASP-25 – stars: individual: WASP-26.

1 INTRODUCTION

Whilst there are over 1000 extrasolar planets now known, much of our understanding of these objects rests on those which transit their parent star. For these exoplanets only is it possible to measure their radius and true mass, allowing the determination of their surface gravity and density, and thus inference of their internal structure and formation processes.

A total of 1137[1] transiting extrasolar planets (TEPs) are now known, but only a small fraction of these have high-precision measurements of their physical properties. Of these 1150 planets, 58 have mass and radius measurements to 5 per cent precision, and only eight to 3 per cent precision.

The two main limitations to the high-fidelity measurements of the masses and radii of TEPs are the precision of spectroscopic radial velocity (RV) measurements (mainly affecting objects discovered using the *CoRoT* and *Kepler* satellites) and the quality of the

★Based on data collected by MiNDSTEp with the Danish 1.54 m telescope at the ESO La Silla Observatory.

†E-mail: astro.js@keele.ac.uk
‡Royal Society University Research Fellow.

[1] Data taken from the Transiting Extrasolar Planet Catalogue (TEPCat) available at http://www.astro.keele.ac.uk/jkt/tepcat/ on 2014/07/16.

transit light curves (for objects discovered via ground-based facilities). Whilst the former problem is intractable with current instrumentation, the latter problem can be solved by obtaining high-precision transit light curves of TEP systems which are bright enough for high-precision spectroscopic observations to be available.

We are therefore undertaking a project to characterize bright TEPs visible from the Southern hemisphere, using the 1.54 m Danish Telescope in defocussed mode. In this work, we present transit light curves of three targets discovered by the SuperWASP project (Pollacco et al. 2006). From these, and published spectroscopic analyses, we measure their physical properties and orbital ephemerides to high precision.

1.1 WASP-24

This planetary system was discovered by Street et al. (2010) and consists of a Jupiter-like planet (mass $1.2M_{\rm Jup}$ and radius $1.3R_{\rm Jup}$) on a circular orbit around a late-F star (mass 1.2 $\rm M_\odot$ and radius 1.3 $\rm R_\odot$) every 2.34 d. The comparatively short orbital period and hot host star means that WASP-24 b has a high equilibrium temperature of 1800 K. Street et al. (2010) obtained photometry of eight transits, of which three were fully observed, from the Liverpool, Faulkes North and Faulkes South telescopes (LT, FTN and FTS). The nearest star to WASP-24 (21.2 arcsec) was found to be an eclipsing binary system with 0.8 mag deep eclipses on a possible period of 1.156 d.

Simpson et al. (2011) obtained high-precision RVs of one transit using the HARPS spectrograph. From modelling of the Rossiter–McLaughlin (RM) effect (McLaughlin 1924; Rossiter 1924), they found a projected spin–orbit alignment angle $\lambda = -4\overset{\circ}{.}7 \pm 4\overset{\circ}{.}0$. This is consistent with WASP-24 b having zero orbital obliquity.

Smith et al. (2012) presented observations of two occultations (at 3.6 and 4.5 μm) with the *Spitzer* space telescope. These data were used to constrain the orbital eccentricity to be $e < 0.039$ (3σ), but were not sufficient to determine whether WASP-24 b possesses an atmospheric inversion layer. Smith et al. (2012) also observed one transit in the Strömgren u and y passbands with the BUSCA multiband imager (see Southworth et al. 2012) and provided new measurements of the physical properties of the system.

Knutson et al. (2014) studied the orbital motion of WASP-24 over 3.5 yr using high-precision RVs from multiple telescopes. They found no evidence for orbital eccentricity or for a long-term drift attributable to a third body in the system. Finally, Sada et al. (2012) obtained one transit light curve of WASP-24, and spectral analyses of the host star have been performed by Torres et al. (2012) and Mortier et al. (2013).

1.2 WASP-25

WASP-25 (Enoch et al. 2011) is a comparatively unstudied system containing a low-density transiting planet (mass $0.6M_{\rm Jup}$, radius $1.2R_{\rm Jup}$) orbiting a solar-like star (mass 1.1 $\rm M_\odot$, radius 0.9 $\rm R_\odot$) every 3.76 d. Their follow-up observations included two transits, one observed with FTS and one with the Euler telescope. Brown et al. (2012) observed one transit with HARPS, detecting the RM effect and finding $\lambda = 14\overset{\circ}{.}6 \pm 6\overset{\circ}{.}7$. They deduced that this is consistent with an aligned orbit, using the Bayesian Information Criterion.

Maxted, Koen & Smalley (2011) measured the effective temperature ($T_{\rm eff}$) of WASP-25 A using the infrared flux method. Mortier et al. (2013) obtained the spectral parameters of the star from high-resolution spectroscopy.

1.3 WASP-26

WASP-26 was discovered by Smalley et al. (2010) and contains a typical hot Jupiter (mass $1.0M_{\rm Jup}$, radius $1.2R_{\rm Jup}$) orbiting a G0 V star (mass 1.1 $\rm M_\odot$, radius 1.3 $\rm R_\odot$) in a circular 2.75 d orbit. WASP-26 has a common-proper-motion companion at 15 arcsec which is roughly 2.5 mag fainter than the planet host star. Smalley et al. (2010) observed one transit of WASP-26 with FTS and one with a large scatter with FTN.

Anderson et al. (2011) obtained high-precision RVs using HARPS through one transit of WASP-26, but their data were insufficient to allow detection of the RM effect. They also observed a transit with a 35 cm telescope; the data are too scattered to be useful for the current work. Albrecht et al. (2012) observed a spectroscopic transit using Keck/HIRES and made a low-confidence detection of the RM effect resulting in $\lambda = -34^{\circ}{}^{+36^{\circ}}_{-26^{\circ}}$.

Mahtani et al. (2013) observed two occultations, at 3.6 and 4.5 μm, using *Spitzer*. They were unable to distinguish whether the planet has an atmosphere with or without a thermal inversion, but could conclude that the orbit was likely circular with $e < 0.04$ at 3σ confidence. Mahtani et al. (2013) also presented light curves of a transit taken in the g, r and i filters, using BUSCA.

Maxted et al. (2011) measured the $T_{\rm eff}$ of WASP-26 A using the infrared flux method. Mortier et al. (2013) determined the atmospheric parameters of the star from high-resolution spectroscopy.

2 OBSERVATIONS AND DATA REDUCTION

2.1 Observations

All observations were taken with the DFOSC (Danish Faint Object Spectrograph and Camera) instrument mounted on the 1.54 m Danish Telescope at ESO La Silla, Chile. This setup yields a field of view of 13.7 arcmin ×13.7 arcmin at a plate scale of 0.39 arcsec pixel^{-1}. We defocussed the telescope in order to improve the precision and efficiency of our observations (see Southworth et al. 2009a for detailed signal-to-noise calculations). We windowed the CCD in order to lower the amount of observing time lost to readout. The autoguider was used to maintain pointing, resulting in a drift of no more than five pixels through individual observing sequences. Most nights were photometric. An observing log is given in Table 1 and the final light curves are plotted in Fig. 1. The data were taken through either a Bessell R or Bessell I filter.

Two of our light curves do not have full coverage of a transit. We missed the start of the transit of WASP-24 on 2013/05/22 due to telescope pointing restrictions. Parts of the transit of WASP-25 on 2010/06/13 were lost to technical problems and then cloud. Finally, data for one transit of WASP-24 and one of WASP-26 extend only slightly beyond egress as high winds demanded closure of the telescope dome.

2.2 Telescope and instrument upgrades

Up to and including the 2011 observing season, the CCD in DFOSC was operated with a gain of ∼1.4 ADU per e$^-$, a readout noise of ∼4.3 e$^-$ and 16-bit digitization. As part of a major overhaul of the Danish telescope, a new CCD controller was installed for the 2012 season. The CCD is now operated with a much higher gain (∼4.2 ADU per e$^-$) and 32-bit digitization, so the readout noise (∼5.0 e$^-$) is much smaller relative to the number of ADU recorded for a particular star. The onset of saturation with the new CCD controller is at roughly 680 000 ADU (Andersen, private communication).

Table 1. Log of the observations presented in this work. N_{obs} is the number of observations, T_{exp} is the exposure time, T_{dead} is the dead time between exposures, 'Moon illum.' is the fractional illumination of the Moon at the mid-point of the transit and N_{poly} is the order of the polynomial fitted to the out-of-transit data. The aperture radii are target aperture, inner sky and outer sky, respectively.

Target	Date of first obs	Start time (UT)	End time (UT)	N_{obs}	T_{exp} (s)	T_{dead} (s)	Filter	Airmass	Moon illum.	Aperture radii (pixels)	N_{poly}	Scatter (mmag)
WASP-24	2010 06 16	00:29	06:08	129	120	39	*R*	1.36 → 1.17 → 2.38	0.275	29 45 80	2	0.454
WASP-24	2011 05 06	02:29	08:07	125	120	42	*R*	1.47 → 1.17 → 1.77	0.085	30 40 70	2	0.745
WASP-24	2011 06 29	00:03	05:03	113	120	40	*R*	1.25 → 1.17 → 2.08	0.056	29 40 70	2	0.959
WASP-24	2013 05 22	01:47	05:14	123	80–100	9	*I*	1.37 → 1.17 → 1.26	0.871	16 28 60	1	0.825
WASP-24	2013 05 29	00:58	05:15	151	80–100	16	*I*	1.46 → 1.17 → 1.33	0.785	17 26 50	1	1.061
WASP-24	2013 06 05	00:51	05:48	149	100	20	*I*	1.37 → 1.17 → 1.63	0.111	22 30 50	1	1.185
WASP-25	2010 06 13	23:02	02:42	72	100–120	41	*R*	1.04 → 1.00 → 1.63	0.035	28 40 65	1	0.494
WASP-25	2013 05 03	02:12	08:00	139	112–122	25	*R*	1.01 → 1.00 → 2.41	0.417	20 32 70	2	1.040
WASP-25	2013 06 05	23:58	05:17	173	100	9	*R*	1.02 → 1.00 → 2.07	0.058	22 35 70	1	0.663
WASP-26	2012 09 17	02:26	05:42	222	31–60	46	*I*	1.33 → 1.03 → 1.04	0.017	20 50 80	1	1.201
WASP-26	2013 08 22	03:39	08:17	124	120	14	*I*	1.43 → 1.03 → 1.45	0.980	18 50 80	1	0.689
WASP-26	2013 09 02	04:11	09:29	153	100	25	*I*	1.17 → 1.03 → 1.47	0.101	20 55 80	2	0.621
WASP-26	2013 09 12	03:36	09:16	393	30	25	*I*	1.15 → 1.03 → 1.69	0.567	14 50 80	1	1.029

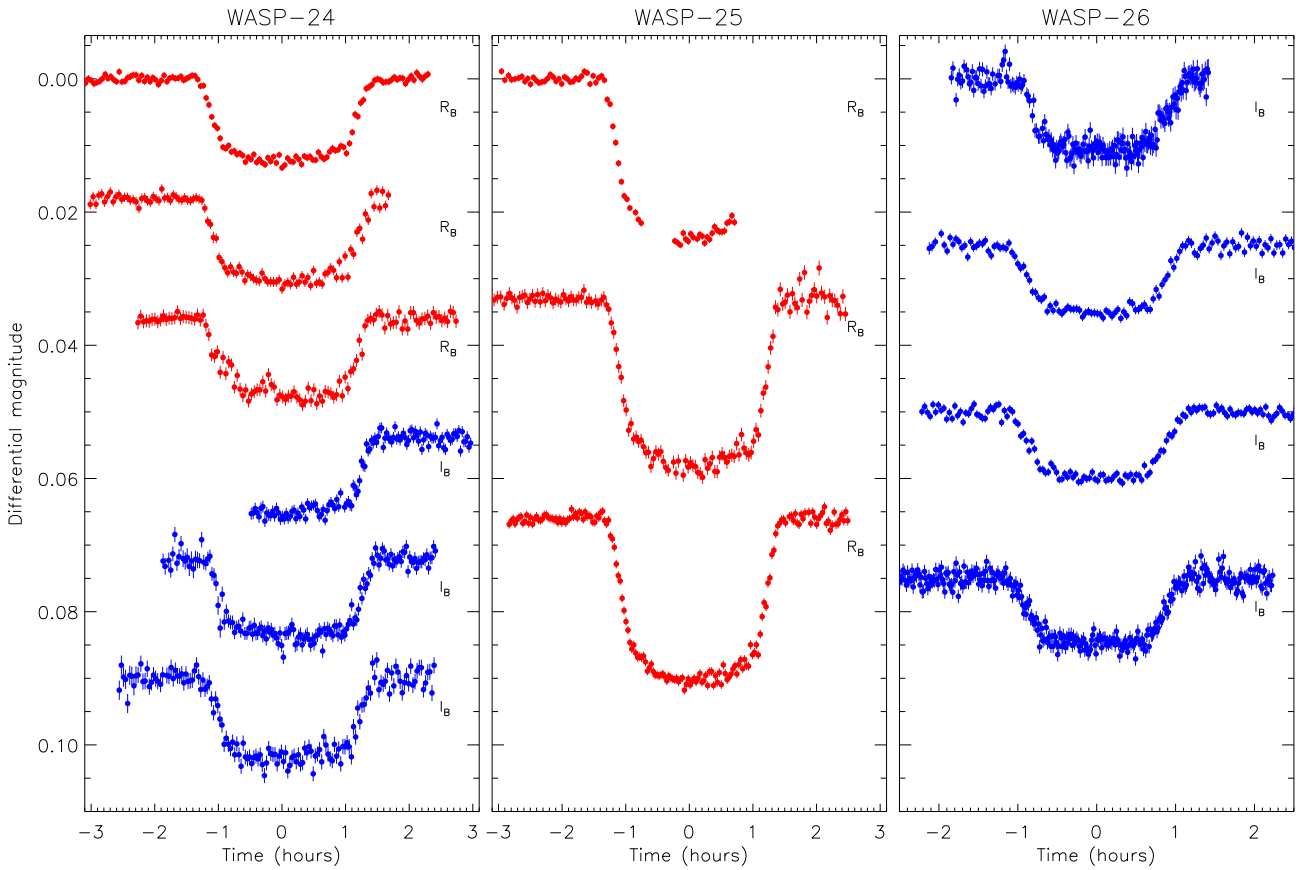

Figure 1. Light curves presented in this work, in the order they are given in Table 1. Times are given relative to the mid-point of each transit, and the filter used is indicated. Blue and red filled circles represent observations through the Bessell *R* and *I* filters, respectively.

For the current project, we aimed for a maximum pixel count rate of between 250 000 and 350 000 ADU, in order to ensure that we stayed well below the threshold for saturation. The effect of this is that less defocussing was required due to the greater dynamic range of the CCD controller, so the object apertures for the 2012 and 2013 season are smaller than those for the 2010 and 2011 seasons. The lesser importance of readout noise also means that the CCD could be read out more quickly, so the newer data have a higher observational cadence. These effects are visible in Table 1.

2.3 Aperture photometry

The data were reduced using the DEFOT pipeline, which is written in IDL[2] and uses routines from the ASTROLIB library.[3] DEFOT

[2] The acronym IDL stands for Interactive Data Language and is a trademark of ITT Visual Information Solutions. For further details see http://www.ittvis.com/ProductsServices/IDL.aspx.

[3] The ASTROLIB subroutine library is distributed by NASA. For further details see http://idlastro.gsfc.nasa.gov/.

has undergone several modifications since its first use (Southworth et al. 2009a) and we review these below.

The first modification is that pointing changes due to telescope guiding errors are measured by cross-correlating each image against a reference image, using the following procedure. First, the image in question and the reference image are each collapsed in the x and y directions, whilst avoiding areas affected by a significant number of bad pixels. The resulting one-dimensional arrays are each divided by a robust polynomial fit, where the quantity minimized is the mean-absolute-deviation rather than the usual least squares. The x and y arrays are then cross-correlated, and Gaussian functions are fitted to the peaks of the cross-correlation functions in order to measure the spatial offset. The photometric apertures are then shifted by the measured amounts in order to track the motion of the stellar images across the CCD.

This modification has been in routine use since our analysis of WASP-2 (Southworth et al. 2010). It performs extremely well as long as there is no field rotation during observations. It is much easier to track offsets between entire images rather than the alternative of following the positions of individual stars in the images, as the point spread functions (PSFs) are highly non-Gaussian so their centroids are difficult to measure.[4]

Aperture photometry was performed by the DEFOT pipeline using the APER algorithm from the ASTROLIB implementation of the DAOPHOT package (Stetson 1987). We placed the apertures by hand on the target and comparison stars, and tried a wide range of sizes for all three apertures. For our final light curves, we used the aperture sizes which yielded the most precise photometry, measured versus a fitted transit model (see below). We find that different choices of aperture size do affect the photometric precision but do not yield differing transit shapes. The aperture sizes are reported in Table 1.

2.4 Bias and flat-field calibrations

Master bias and flat-field calibration frames were constructed for each observing season, by median-combining large numbers of individual bias and twilight-sky images. For each observing sequence, we tested whether their inclusion in the analysis produces photometry with a lower scatter. Inclusion of the master bias image was found to have a negligible effect in all cases, whereas using a master flat-field can either aid or hinder the quality of the resulting photometry. It only led to a significant improvement in the scatter of the light curve for the observation of WASP-24 on 2010/06/16. It is probably not a coincidence that this data set yielded the least scattered light curve either with or without flat-fielding.

We attribute the divergent effects of flat-fielding to the varying relative importance of the advantages and disadvantages of the calibration process. The main advantage is that variations in pixel efficiency, which occur on several spatial scales, can be compensated for. Small-scale variations (i.e. variations between adjacent pixels) average down to a low level as our defocussed PSFs cover of the order of 1000 pixels, so this effect is unimportant. Large-scale variations (e.g. differing illumination levels over the CCD) are usually dealt with by autoguiding the telescope – flat-fielding is in general more important for cases when the telescope tracking is poor. The disadvantages of the standard approach to flat-fielding are (1) the master flat-field image has Poisson noise which is propagated into the science images; (2) pixel efficiency depends on wavelength, so observations of red stars are not properly calibrated using observations of a blue twilight sky; (3) pixel efficiency depends on the number of counts, which is in general different for the science and the calibration observations.

[4] See Nikolov et al. (2013) for one way of determining the centroid of a highly defocussed PSF.

Table 2. Excerpts of the light curves presented in this work. The full data set will be made available at the CDS.

Target	Filter	BJD(TDB)	Diff. mag.	Uncertainty
WASP-24	*R*	2455364.525808	−0.00079	0.00054
WASP-24	*R*	2455364.527590	−0.00018	0.00053
WASP-24	*R*	2455364.529430	−0.00001	0.00055
WASP-25	*R*	2455361.464729	−0.00113	0.00052
WASP-25	*R*	2455361.466882	0.00019	0.00051
WASP-25	*R*	2455361.469289	−0.00049	0.00051
WASP-26	*I*	2456187.608599	−0.00016	0.00101
WASP-26	*I*	2456187.609444	−0.00161	0.00103
WASP-26	*I*	2456187.611111	0.00316	0.00103

2.5 Light-curve generation

The instrumental magnitudes of the target and comparison stars were converted into differential-magnitude light curves normalized to zero magnitude outside transit, using the following procedure. For each observing sequence, an ensemble comparison star was constructed by adding the fluxes of all good comparison stars with weights adjusted to give the lowest possible scatter for the data taken outside transit. The normalization was performed by fitting a polynomial to the out-of-transit data points. We used a first-order polynomial when possible, as this cannot modify the shape of the transit, but switched to a second-order polynomial when the observations demanded. The weights of the comparison stars and the coefficients were optimized simultaneously to yield the final differential-magnitude light curve. The order of the polynomial used for each data set is given in Table 1.

In the original version of the DEFOT pipeline, the optimization of the weights and coefficients was performed using the IDL AMOEBA routine, which is an implementation of the downhill simplex algorithm of Nelder & Mead (1965). We have found that this routine can suffer from irreproducibility of results, primarily as it is prone to getting trapped in local minima. We have therefore modified DEFOT to use the MPFIT implementation of the Levenberg–Marquardt algorithm (Markwardt 2009). We find the fitting process to be much faster and more reliable when using MPFIT compared to using AMOEBA.

The timestamps for the data points have been converted to the BJD(TDB) time-scale (Eastman, Siverd & Gaudi 2010). Manual time checks were obtained for several frames and the FITS file timestamps were confirmed to be on the UTC system to within a few seconds. The timings therefore appear not to suffer from the same problems as previously found for WASP-18 and suspected for WASP-16 (Southworth et al. 2009b, 2013). The light curves are shown in Fig. 1. The reduced data are enumerated in Table 2 and will be made available at the CDS.[5]

3 HIGH-RESOLUTION IMAGING

For each object, we obtained well-focused images with DFOSC in order to check for faint nearby stars whose light might have

[5] http://vizier.u-strasbg.fr/

contaminated that from our target star. Such objects would dilute the transit and cause us to underestimate the radius of the planet (Daemgen et al. 2009). The worst-case scenario is a contaminant which is an eclipsing binary, as this would render the planetary nature of the system questionable.

For WASP-24, we find nearby stars at 43 and 55 pixels (16.8 and 21.5 arcsec), which are more than 7.6 and 4.5 mag fainter than the target star in the *R* filter. Precise photometry is not available for the focused images as WASP-24 itself is saturated to varying degrees. We estimate that the star at 43 pixels contributes less than 0.01 per cent of the flux in the inner aperture of WASP-24, which is much too small to affect our results. The star at 55 pixels is an eclipsing binary (see Section 7) but its PSF was always clearly separated from that of WASP-24 so it also contributes an unmeasurably small amount of flux to the inner aperture of WASP-24.

For WASP-25, the nearest star is at 94 pixels and is 5.36 mag fainter than our target. The inner aperture for WASP-25 is significantly smaller than this distance, so the presence of the nearby star has a negligible effect on our photometry. For WASP-26, there is a known star which is 39 pixels (15.2 arcsec) away from the target and 2.55 mag fainter in our images. The object and sky apertures in Section 2 were selected such that this star was in no-man's land between them, and thus had an insignificant effect on our photometry.

In order to search for stars which are very close to our target systems, we obtained high-resolution images of all three targets using the Lucky Imager (LI) mounted on the Danish telescope. The LI uses an Andor 512 × 512 pixel electron-multiplying CCD, with a pixel scale of 0.09 arcsec pixel^{-1} and a field of view of 45 arcsec × 45 arcsec. The data were reduced using a dedicated pipeline and the best 2 per cent of images were stacked together to yield combined images whose PSF is smaller than the seeing limit. A long-pass filter was used, resulting in a response which approximates that of SDSS $i + z$ (Skottfelt et al. 2013). Exposure times of 120, 220 and 109 s were used for WASP-24, WASP-25 and WASP-26, respectively. The LI observations are thus shallower than the focused DFOSC images, but have a better resolution. A detailed examination of different high-resolution imaging approaches was recently given by Lillo-Box, Barrado & Bouy (2014).

The central parts of the images are shown in Figs 2 and 3. The image for WASP-24 has a PSF full width at half-maximum of 4.1 pixels in *x* (pixel column) and 4.8 pixels in *y* (pixel row), corresponding to 0.37 arcsec × 0.43 arcsec. The image of WASP-25 is nearly as good (4.2 × 5.3 pixels), and that for WASP-26 is better (3.8 × 4.4 pixels). None of the images show any stars which were undetected on our focused DFOSC observations, so we find no evidence for contaminating light in the PSFs of the targets. There is a suggestion of a very faint star north-east of WASP-24, but this was not confirmed

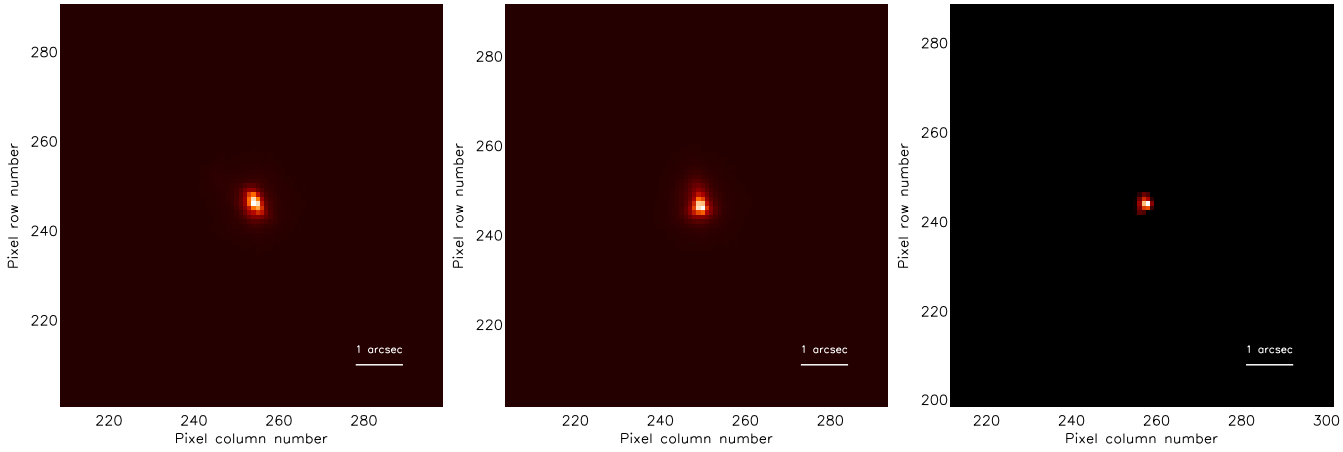

Figure 2. High-resolution Lucky Imaging observations of WASP-24 (left), WASP-25 (middle) and WASP-26 (right). In each case, an image covering 8 arcsec × 8 arcsec and centred on our target star is shown. A bar of length 1 arcsec is superimposed in the bottom right of each image. The flux scale is linear. Each image is a sum of the best 2 per cent of the original images, so the effective exposure times are 2.4, 4.4 and 2.1 s, respectively.

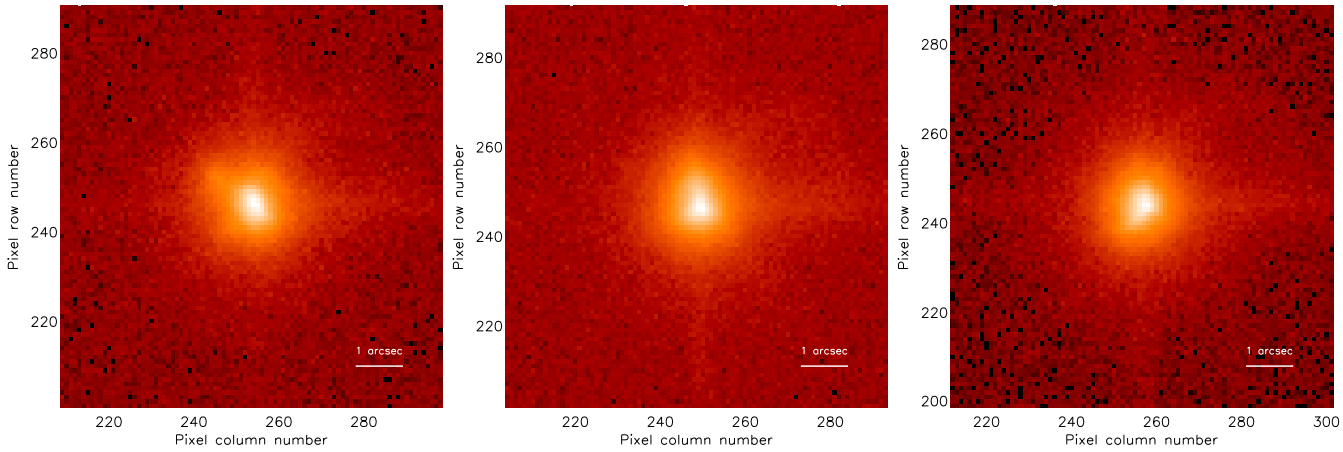

Figure 3. Same as Fig. 2, except that the flux scale is logarithmic so faint stars are more easily identified.

Table 3. Times of minimum light and their residuals versus the ephemeris derived in this work.

Target	Time of minimum (BJD/TDB)	Uncertainty (d)	Cycle number	Residual (d)	Reference
WASP-24	2455081.38018	0.000 17	−259.0	0.000 44	Street et al. (2010)
WASP-24	2455308.47842	0.001 51	−162.0	0.000 17	Ayiomamitis (TRESCA)
WASP-24	2455308.48020	0.001 63	−162.0	0.001 95	Brát (TRESCA)
WASP-24	2455322.52496	0.000 74	−156.0	−0.000 61	This work (BUSCA *u* band)
WASP-24	2455322.52498	0.000 49	−156.0	−0.000 59	This work (BUSCA *y* band)
WASP-24	2455364.66718	0.000 24	−138.0	−0.000 38	This work (Danish Telescope)
WASP-24	2455687.75622	0.000 38	0.0	0.000 06	This work (Danish Telescope)
WASP-24	2455701.80338	0.000 49	6.0	−0.000 11	Sada et al. (2012)
WASP-24	2455741.60468	0.000 52	23.0	0.000 42	This work (Danish Telescope)
WASP-24	2456010.84351	0.000 52	138.0	−0.001 25	Wallace et al. (TRESCA)
WASP-24	2456010.84412	0.000 62	138.0	−0.000 64	Wallace et al. (TRESCA)
WASP-24	2456408.85005	0.002 57	308.0	−0.002 40	Garlitz (TRESCA)
WASP-24	2456441.63058	0.000 42	322.0	0.001 02	This work (Danish Telescope)
WASP-24	2456448.65324	0.000 49	325.0	0.000 02	This work (Danish Telescope)
WASP-25	2455274.99726	0.000 21	−163.0	0.000 15	Enoch et al. (2011)
WASP-25	2455338.99804	0.000 75	−146.0	−0.001 23	Curtis (TRESCA)
WASP-25	2455659.01066	0.001 18	−61.0	0.000 61	Curtis (TRESCA)
WASP-25	2455677.83276	0.000 78	−56.0	−0.001 45	Evans (TRESCA)
WASP-25	2456415.74114	0.000 21	140.0	−0.000 28	This work
WASP-25	2456430.80140	0.000 63	144.0	0.000 65	Evans (TRESCA)
WASP-25	2456449.62499	0.000 12	149.0	0.000 08	This work
WASP-26	2455123.63867	0.000 70	−259.0	−0.000 86	Smalley et al. (2010)
WASP-26	2455493.02404	0.001 83	−125.0	0.000 48	Curtis (TRESCA)
WASP-26	2456187.68731	0.000 43	127.0	0.001 25	This work
WASP-26	2456526.74716	0.000 41	250.0	−0.000 36	This work
WASP-26	2456537.77389	0.000 36	254.0	−0.000 02	This work
WASP-26	2456548.79992	0.000 38	258.0	−0.000 38	This work

by a repeat image. If present, its brightness is insufficient to have a significant effect on our analysis.

4 ORBITAL PERIOD DETERMINATION

Our first step was to improve the measured orbital ephemerides of the three TEPs using our new data. Each of our light curves was fitted using the JKTEBOP code (see below) and their error bars were rescaled to give a reduced χ^2 of $\chi^2_\nu = 1.0$ versus the fitted model. This step is necessary as the uncertainties from the APER algorithm tend to be underestimated. We then fitted each revised data set to measure the transit mid-points and ran Monte Carlo simulations to estimate the uncertainties in the mid-points. The two transits with only partial coverage were not included in this analysis, as they yield less reliable timings (e.g. Gibson et al. 2009).

We have collected additional times of transit mid-point from literature sources. Those from the discovery papers (Smalley et al. 2010; Street et al. 2010; Enoch et al. 2011) are on the UTC time-scale (Anderson, private communication) so we converted them to TDB to match our own results. We used the timings from our own fits to the BUSCA light curves presented by Smith et al. (2012) for WASP-24.

We also collated minimum timings from the Exoplanet Transit Database[6] (Poddaný, Brát & Pejcha 2010), which provides data and times of minimum from amateur observers affiliated with TRESCA.[7] We retained only those timing measurements based on light curves where all four contact points of the transit are easily identifiable by eye. We assumed that the times were all on the UTC time-scale and converted them to TDB.

For each object, we fitted the times of mid-transit with straight lines to determine new linear orbital ephemerides. Table 3 gives all transit times plus their residual versus the fitted ephemeris. The uncertainties have been increased to force $\chi^2_\nu = 1.0$, E gives the cycle count versus the reference epoch and the bracketed numbers show the uncertainty in the final digit of the preceding number.

The revised ephemeris for WASP-24 is

$$T_0 = \mathrm{BJD(TDB)}\ 2\,455\,687.75616(16) + 2.3412217(8) \times E,$$

where the error bars have been inflated to account for $\chi^2_\nu = 1.75$. We have adopted one of our timings from the 2011 season as the reference epoch. This is close to the mid-point of the available data so the covariance between the orbital period and the time of reference epoch is small.

Our orbital ephemeris for WASP-25 is

$$T_0 = \mathrm{BJD(TDB)}\ 2\,455\,888.66484(13) + 3.7648327(9) \times E,$$

accounting for $\chi^2_\nu = 1.21$. We have adopted a reference epoch midway between our 2013 data and the timing from the discovery paper.

The new orbital ephemeris for WASP-26 is

$$T_0 = \mathrm{BJD(TDB)}\ 2\,455\,837.59821(44) + 2.7565972(19) \times E,$$

accounting for $\chi^2_\nu = 1.40$ and using a reference epoch in mid-2011. The main contributor to the χ^2_ν is our transit from 2012, which was observed under conditions of poor sky transparency. Whilst a parabolic ephemeris provides a formally better fit to the transit times, this improvement is due almost entirely to our 2012 transit so is not reliable.

[6] The Exoplanet Transit Database (ETD) can be found at http://var2.astro.cz/ETD/credit.php

[7] The TRansiting ExoplanetS and CAndidates (TRESCA) website can be found at http://var2.astro.cz/EN/tresca/index.php

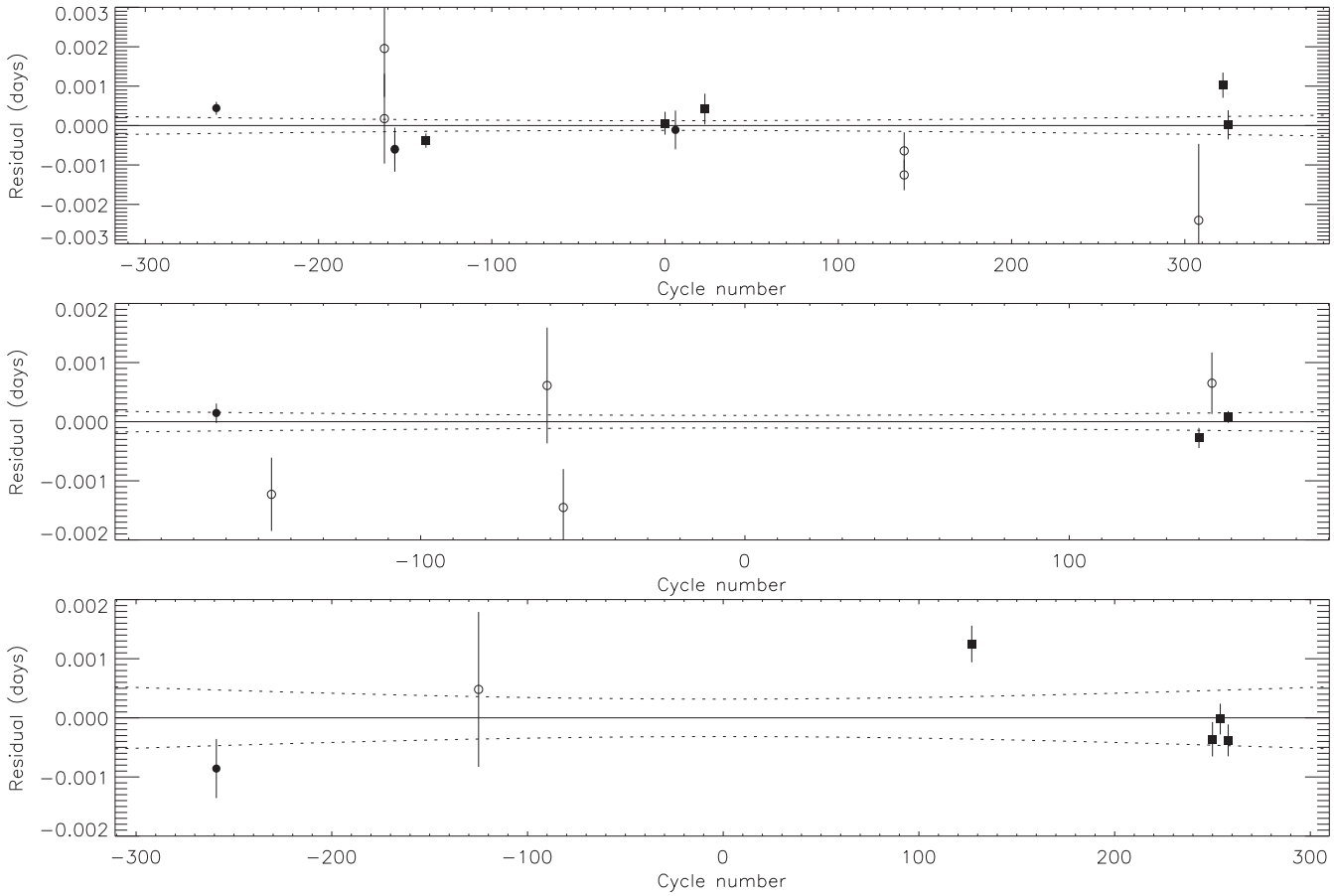

Figure 4. Plot of the residuals of the timings of mid-transit versus a linear ephemeris, for WASP-24 (top), WASP-25 (middle) and WASP-26 (bottom). The results from this work are shown using filled squares, and from amateur observers with open circles. All other timings are shown by filled circles. The dotted lines show the 1σ uncertainty in the ephemeris as a function of cycle number. The error bars have been scaled up to force $\chi^2_\nu = 1.0$.

Fig. 4 shows the residuals versus the linear ephemeris for each of our three targets. No transit timing variations are discernable by eye, and there are insufficient timing measurements to perform a quantitative search for such variations. Our period values for all three systems are consistent with previous measurements but are significantly more precise due to the longer temporal baseline of the available transit timings.

5 LIGHT-CURVE ANALYSIS

We have analysed the light curves using the *Homogeneous Studies* methodology (see Southworth 2012 and references therein), which utilizes the JKTEBOP[8] code (Southworth, Maxted & Smalley 2004) and the NDE model (Nelson & Davis 1972; Popper & Etzel 1981). This represents the star and planet as spheres for the calculation of eclipse shapes and as biaxial spheroids for proximity effects.

The fitted parameters of the model for each system were the fractional radii of the star and planet (r_A and r_b), the orbital inclination (i), limb darkening (LD) coefficients and the reference time of mid-transit. The fractional radii are the ratio between the true radii and the semimajor axis: $r_{A,b} = \frac{R_{A,b}}{a}$. They were expressed as their sum and ratio, $r_A + r_b$ and $k = \frac{r_b}{r_A}$, because these two quantities are more weakly correlated. The orbital period was held fixed at the value found in Section 4. We assumed a circular orbit for each system based on the case histories given in Section 1.

Whilst the light curves had already been rectified to zero differential magnitude outside transit, the uncertainties in this process need to be propagated through subsequent analyses. This effect is relatively unimportant for transits with plenty of data before ingress and after egress, as the rectification polynomial is well defined and needs only to be interpolated to the data within transit. It is, however, crucial for partial transits as the rectification polynomial is defined on only a short stretch of data on one side of the transit, which then needs to be extrapolated to all in-transit data. JKTEBOP was therefore modified to allow multiple polynomials to be specified, each operating on only a subset of data within a specific time interval. This allowed multiple light curves to be modelled simultaneously but subject to independent polynomial fits to the out-of-transit data. For each transit, we included as fitted parameters the coefficients of a polynomial of order given in Table 1. We found that the coefficients of the polynomials did not exhibit strong correlations against the other model parameters: the correlation coefficients are normally less than 0.4.

LD was accounted for by each of five LD laws (see Southworth 2008), with the linear coefficients either fixed at

[8] JKTEBOP is written in FORTRAN77 and the source code is available at http://www.astro.keele.ac.uk/jkt/codes/jktebop.html.

theoretically predicted values[9] or included as fitted parameters. We did not calculate fits for both LD coefficients in the four bi-parametric laws as they are very strongly correlated (Carter et al. 2008; Southworth 2008). The non-linear coefficients were instead perturbed by ±0.1 on a flat distribution during the error analysis simulations, in order to account for imperfections in the theoretically predicted coefficients.

Error estimates for the fitted parameters were obtained in several ways. We ran solutions using different LD laws, and also calculated error bars using residual-permutation and Monte Carlo algorithms (Southworth 2008). The final value for each parameter is the unweighted mean of the four values from the solutions using the two-parameter LD laws. Its error bar was taken to be the larger of the Monte Carlo or residual-permutation alternatives, with an extra contribution to account for variations between solutions with the different LD laws. Tables of results for each light curve, including our reanalysis of published data, can be found in the Supplementary Information.

5.1 Results for WASP-24

For WASP-24, we divided our data into two data sets, one for the *R* and one for the *I* filters. For each we calculated solutions for all five LD laws under two scenarios: both LD coefficients fixed ('LD-fixed'), and the linear coefficient fitted whilst the non-linear coefficient was fixed but then perturbed in the error analysis simulations ('LD-fit/fix'). The two data sets give consistent results and show no signs of red noise (the Monte Carlo error bars were similar to or larger than the residual-permutation error bars).

We also modelled published transit light curves of WASP-24. The discovery paper (Street et al. 2010) presented two light curves which covered complete transits, one from the RISE instrument on the LT and one using Merope on the FTN. The RISE data were first binned by a factor of 10 from 3454 to 346 data points to lower the required CPU time. Sada et al. (2012) observed one transit in the *J* band with the KPNO 2.1 m telescope. Smith et al. (2012) obtained photometry of one transit simultaneously in the Strömgren *u* and *y* bands.

We found that red noise was strong in the RISE and KPNO data (see Fig. 5) so the results from these data sets were not included in our final values. The *u*-band data gave exceptionally uncertain results so we also discounted this data set. The photometric results from the LD-fit/fix cases for the remaining four data sets were combined according to weighted means, to obtain the final photometric parameters of WASP-24 (Table 4). We also checked what the values would be had we not rejected any combination of the three least reliable data sets, and found changes of less than half the error bars in all cases.

Table 4 also shows a comparison between our values and literature results. We note that the two previous publications gave inconsistent results (see in particular the respective values for *k*) despite being based on much of the same data. This implies that their error estimates were optimistic. To obtain final values for the photometric parameters of WASP-24, we have calculated the weighted mean of those from individual data sets. The results found in the current work are based on more extensive data and analysis, and should be preferred over previous values.

[9] Theoretical LD coefficients were obtained by bilinear interpolation to the host star's $T_{\rm eff}$ and $\log g$ using the JKTLD code available from http://www.astro.keele.ac.uk/jkt/codes/jktld.html

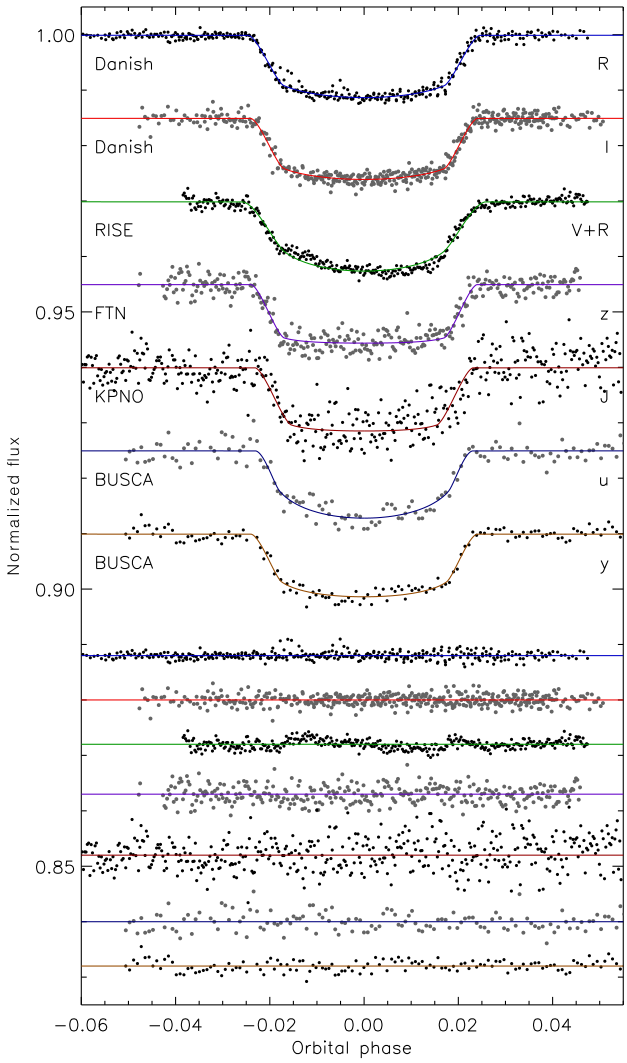

Figure 5. The phased light curves of WASP-24 analysed in this work, compared to the JKTEBOP best fits. The residuals of the fits are plotted at the base of the figure, offset from unity. Labels give the source and passband for each data set. The polynomial baseline functions have been removed from the data before plotting.

5.2 Results for WASP-25

Our three transits were all taken in the Bessell *R* band so were modelled together. We found that red noise was not important and that the data contained sufficient information to fit for the linear LD coefficient. The best fits are plotted in Fig. 6.

Enoch et al. (2011) obtained two transit light curves of WASP-25 in their initial characterization of this object, one from FTS with the Spectral camera and one from the Swiss Euler telescope with EulerCam. For both data sets, we have adopted the LD-fit/fix values. The FTS data have significant curvature outside transit, implying that a quadratic baseline should be included. If this is done, then $r_{\rm A} + r_{\rm b}$ and k become smaller by approximately 1σ and i greater by 1.5σ, yielding the values in Table 5. This change is significantly larger than the error bars quoted by Enoch et al. (2011), which are based primarily on the FTS and the less precise Euler data.

Table 4. Parameters of the fit to the light curves of WASP-24 from the JKTEBOP analysis (top). The final parameters are given in bold and the parameters found by other studies are shown (below). Quantities without quoted uncertainties were not given by those authors but have been calculated from other parameters which were.

Source	$r_A + r_b$	k	$i(^\circ)$	r_A	r_b
Danish Telescope *R* band	0.1900 ± 0.0057	0.1029 ± 0.0013	83.60 ± 0.50	0.1723 ± 0.0050	0.017 73 ± 0.000 70
Danish Telescope *I* band	0.1805 ± 0.0077	0.1012 ± 0.0013	84.23 ± 0.72	0.1639 ± 0.0068	0.016 59 ± 0.000 86
Street LT/RISE	0.2028 ± 0.0157	0.1080 ± 0.0044	82.85 ± 1.31	0.1830 ± 0.0135	0.019 76 ± 0.002 13
Street FTN	0.1807 ± 0.0138	0.1011 ± 0.0014	84.12 ± 1.21	0.1642 ± 0.0123	0.016 59 ± 0.001 38
Sada KPNO *J* band	0.2146 ± 0.0370	0.1090 ± 0.0063	81.34 ± 2.53	0.1935 ± 0.0327	0.021 08 ± 0.004 33
Smith BUSCA *u* band	0.1556 ± 0.1203	0.0990 ± 0.0061	86.57 ± 3.43	0.1416 ± 0.0212	0.014 01 ± 0.003 12
Smith BUSCA *y* band	0.1766 ± 0.0173	0.1016 ± 0.0032	84.59 ± 1.90	0.1603 ± 0.0156	0.016 30 ± 0.001 89
Final results	**0.1855 ± 0.0042**	**0.1018 ± 0.0007**	**83.87 ± 0.38**	**0.1684 ± 0.0037**	**0.017 13± 0.000 49**
Street et al. (2010)	0.1866	0.1004 ± 0.0006	83.64 ± 0.31	0.1696	0.017 02
Smith et al. (2012)	0.1922	0.1050 ± 0.0006	83.30 ± 0.30	0.1739 ± 0.0033	0.018 26

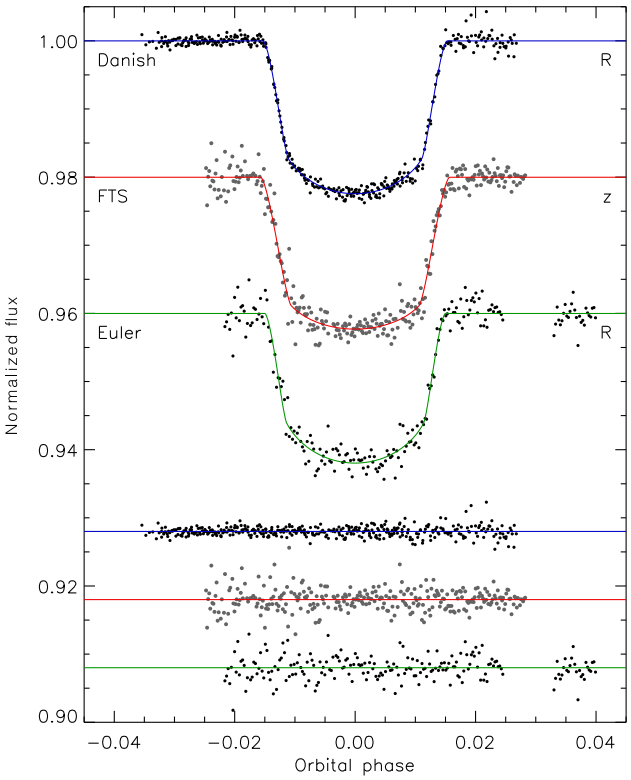

Figure 6. The phased light curves of WASP-25 analysed in this work, compared to the JKTEBOP best fits. The residuals of the fits are plotted at the base of the figure, offset from unity. Labels give the source and passband for each data set. The polynomial baseline functions have been removed from the data before plotting.

5.3 Results for WASP-26

The four transits presented in this work were all taken in the Bessell *I* band, so were modelled together. We found once again that red noise was not important and that the data contained sufficient information to fit for the linear LD coefficient. The best fit is shown in Fig. 7 and the parameter values are given in Table 6.

Smalley et al. (2010) obtained two transit light curves, one each from FTS/Spectral and FTN/Merope. The former has almost no out-of-transit data, and the latter is very scattered. We modelled the FTS light curve here but did not attempt to extract information from the FTN data. We found that the scatter was dominated by white noise and it was not possible to fit for any LD coefficients.

Mahtani et al. (2013) presented photometry of one transit of WASP-26 obtained simultaneously in the *g*, *r* and *i* bands using BUSCA. We modelled these data sets individually. The *g*- and *r*-band data could only support an LD-fixed solution. Red noise was unimportant for *g* and *r* but the residual-permutation error bars were a factor of 2.5 greater than the Monte Carlo error bars for *i*.

Table 6 collects the parameter values found from each light curve. The data from the Danish Telescope are of much higher precision than previous data sets, and yield a solution with larger orbital inclination and smaller fractional radii than obtained in previous studies. Whilst $r_A + r_b$ and i are in overall agreement ($\chi^2_\nu = 1.0$ and 0.8 versus the weighted mean value), k and r_B are not ($\chi^2_\nu = 3.4$ and 1.8). These moderate discrepancies were accounted for by increasing the error bars on the final weighted-mean parameter values, by an amount sufficient to force $\chi^2_\nu = 1.0$.

6 PHYSICAL PROPERTIES

We have measured the physical properties of the three planetary systems using the photometric quantities found in Section 5, published spectroscopic results and five sets of theoretical stellar evolutionary

Table 5. Parameters of the fit to the light curves of WASP-25 from the JKTEBOP analysis (top). The final parameters are given in bold and the parameters found by other studies are shown (below). Quantities without quoted uncertainties were not given by Enoch et al. (2011) but have been calculated from other parameters which were.

Source	$r_A + r_b$	k	$i(^\circ)$	r_A	r_b
Danish Telescope	0.1004 ± 0.0019	0.1384 ± 0.0011	88.33 ± 0.32	0.0882 ± 0.0016	0.012 21 ± 0.000 30
Enoch FTS	0.1072 ± 0.0043	0.1416 ± 0.0026	87.54 ± 0.52	0.0939 ± 0.0036	0.013 28 ± 0.000 67
Enoch Euler	0.1004 ± 0.0067	0.1374 ± 0.0029	88.13 ± 1.37	0.0883 ± 0.0056	0.012 14 ± 0.000 98
Final results	**0.1015 ± 0.0017**	**0.1387 ± 0.0010**	**88.12 ± 0.27**	**0.0891 ± 0.0014**	**0.012 37± 0.000 28**
Enoch et al. (2011)	0.1029	0.1367 ± 0.0007	88.0 ± 0.5	0.09049	0.012 37

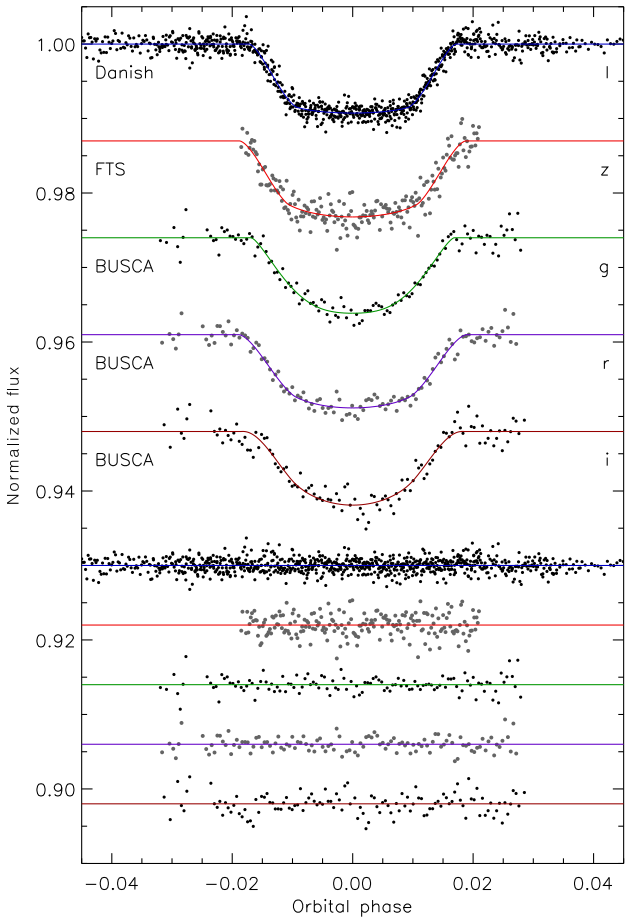

Figure 7. The phased light curves of WASP-26 analysed in this work, compared to the JKTEBOP best fits. The residuals of the fits are plotted at the base of the figure, offset from unity. Labels give the source and passband for each data set. The polynomial baseline functions have been removed from the data before plotting.

models (Claret 2004; Demarque et al. 2004; Pietrinferni et al. 2004; VandenBerg, Bergbusch & Dowler 2006; Dotter et al. 2008). Table 7 gives the spectroscopic quantities adopted from the literature, where K_A denotes the velocity amplitude of the star.

In the case of WASP-24, there are two recent conflicting spectroscopic analyses: Torres et al. (2012) measured $T_{\rm eff} = 6107 \pm 77$ K and $\log g = 4.26 \pm 0.01$ (c.g.s.), whereas Mortier et al. (2013) obtained $T_{\rm eff} = 6297 \pm 58$ K and $\log g = 4.76 \pm 0.17$. We have adopted the former $T_{\rm eff}$ as it agrees with an independent value from Street et al. (2010) and the corresponding $\log g$ is in good agreement with that derived from our own analysis.

Table 7. Spectroscopic properties of the planet host stars used in the determination of the physical properties of the systems.

Target	$T_{\rm eff}$ (K)	$\left[\frac{\rm Fe}{\rm H}\right]$ (dex)	K_A (m s^{-1})	Ref
WASP-24	6107 ± 77	-0.02 ± 0.10	152.1 ± 3.2	1,1,2
WASP-25	5736 ± 50	0.06 ± 0.05	75.5 ± 5.3	3,3,4
WASP-26	6015 ± 55	-0.02 ± 0.09	138 ± 2	5,6,7

References: (1) Torres et al. (2012); (2) Knutson et al. (2014); (3) Mortier et al. (2013); (4) Enoch et al. (2010); (5) Maxted et al. (2011); (6) Smalley et al. (2010); (7) Mahtani et al. (2013).

For each object, we used the measured values of r_A, r_b, i and K_A, and an estimated value of the velocity amplitude of the planet, K_b, to calculate the physical properties of the system. K_b was then iteratively refined to obtain the best agreement between the calculated $\frac{R_A}{a}$ and the measured r_A, and between the spectroscopic $T_{\rm eff}$ and that predicted by the stellar models for the observed $\left[\frac{\rm Fe}{\rm H}\right]$ and the calculated stellar mass (M_A). This was done for a range of ages in order to determine the overall best fit and age of the system. Further details on the method can be found in Southworth (2009). This process was performed for each of the five sets of theoretical stellar models, in order to estimate the systematic error incurred by the use of stellar theory.

The final physical properties of the three planetary systems are given in Table 8. The equilibrium temperatures of the planets were calculated ignoring the effects of albedo and heat redistribution: $T'_{\rm eq} = T_{\rm eff}\sqrt{\frac{r_A}{2}}$. For each parameter which depends on theoretical models, there are five different values, one from using each of the five model sets. In these cases, we give two error bars: the statistical uncertainty (calculated by propagating the random errors via a perturbation analysis) and the systematic uncertainty (the maximum deviation between the final value and the five values from using the different stellar models).

The intermediate results for each set of stellar models are given in Tables A16– A18, along with a comparison to published values. We find that literature values are in generally good agreement with our own, despite being based on much less extensive follow-up photometry (see Figs 5–7) and less precise spectroscopic properties for the host stars. The uncertainties in the radii of WASP-25 b and WASP-26 b are significantly improved by our new results. The uncertainties in the host star mass and semimajor axis measurements for WASP-24 b and WASP-25 b have a significant contribution from the differences in the theoretical model predictions we used, an issue which was not considered in previous studies of these objects.

Table 6. Parameters of the fit to the light curves of WASP-26 from the JKTEBOP analysis (top). The final parameters are given in bold and the parameters found by other studies are shown (below). Quantities without quoted uncertainties were not given by those authors but have been calculated from other parameters which were.

Source	$r_A + r_b$	k	$i(^\circ)$	r_A	r_b
Danish Telescope	0.1584 ± 0.0044	0.0973 ± 0.0008	83.29 ± 0.32	0.1444 ± 0.0040	$0.014\,05 \pm 0.000\,38$
Smalley FTS	0.176 ± 0.011	0.1027 ± 0.0044	82.47 ± 0.63	0.160 ± 0.010	0.0164 ± 0.0016
Mahtani g band	0.1733 ± 0.0089	0.1081 ± 0.0029	82.31 ± 0.53	0.1564 ± 0.0077	0.0169 ± 0.0012
Mahtani r band	0.174 ± 0.017	0.1026 ± 0.0042	82.6 ± 1.2	0.158 ± 0.015	0.0162 ± 0.0016
Mahtani i band	0.184 ± 0.035	0.103 ± 0.032	81.5 ± 2.2	0.166 ± 0.020	0.0172 ± 0.0091
Final results	$\mathbf{0.1649 \pm 0.0040}$	$\mathbf{0.0991 \pm 0.0018}$	$\mathbf{82.83 \pm 0.27}$	$\mathbf{0.1505 \pm 0.0036}$	$\mathbf{0.014\,65 \pm 0.000\,54}$
Smalley et al. (2010)	0.1716	0.101 ± 0.002	82.5 ± 0.5	0.1559	0.015 74
Anderson et al. (2011)	0.1675	0.1011 ± 0.0017	82.5 ± 0.5	0.1521	0.015 38
Mahtani et al. (2013)	0.1661	0.1015 ± 0.0015	82.5 ± 0.5	0.1508	0.015 36

Table 8. Derived physical properties of the three systems. Where two sets of error bars are given, the first is the statistical uncertainty and the second is the systematic uncertainty.

Quantity	Symbol	Unit	WASP-24	WASP-25	WASP-26
Stellar mass	$M_{\rm A}$	$M_\odot$	$1.168 \pm 0.056 \pm 0.050$	$1.053 \pm 0.023 \pm 0.030$	$1.095 \pm 0.043 \pm 0.017$
Stellar radius	$R_{\rm A}$	$R_\odot$	$1.317 \pm 0.036 \pm 0.019$	$0.924 \pm 0.016 \pm 0.009$	$1.284 \pm 0.035 \pm 0.007$
Stellar surface gravity	$\log g_{\rm A}$	c.g.s.	$4.267 \pm 0.021 \pm 0.006$	$4.530 \pm 0.014 \pm 0.004$	$4.260 \pm 0.022 \pm 0.002$
Stellar density	$\rho_{\rm A}$	$\rho_\odot$	0.512 ± 0.034	1.336 ± 0.063	0.517 ± 0.037
Planet mass	$M_{\rm b}$	$M_{\rm Jup}$	$1.109 \pm 0.043 \pm 0.032$	$0.598 \pm 0.044 \pm 0.012$	$1.020 \pm 0.031 \pm 0.011$
Planet radius	$R_{\rm b}$	$R_{\rm Jup}$	$1.303 \pm 0.043 \pm 0.019$	$1.247 \pm 0.030 \pm 0.012$	$1.216 \pm 0.047 \pm 0.006$
Planet surface gravity	$g_{\rm b}$	m s^{-2}	16.19 ± 0.99	9.54 ± 0.80	17.1 ± 1.3
Planet density	$\rho_{\rm b}$	$\rho_{\rm Jup}$	$0.469 \pm 0.042 \pm 0.007$	$0.288 \pm 0.028 \pm 0.003$	$0.530 \pm 0.060 \pm 0.003$
Equilibrium temperature	$T'_{\rm eq}$	K	1772 ± 29	1210 ± 14	1650 ± 24
Safronov number	Θ		$0.0529 \pm 0.0021 \pm 0.0007$	$0.0439 \pm 0.0033 \pm 0.0004$	$0.0607 \pm 0.0026 \pm 0.0003$
Orbital semimajor axis	a	au	$0.036\,35 \pm 0.000\,59 \pm 0.000\,52$	$0.048\,19 \pm 0.000\,35 \pm 0.000\,46$	$0.039\,66 \pm 0.000\,52 \pm 0.000\,21$
Age	τ	Gyr	$2.5\,^{+9.6\ +1.8}_{-1.5\ -2.5}$	$0.1\,^{+5.7\ +0.2}_{-0.1\ -0.0}$	$4.0\,^{+5.7\ +1.4}_{-4.5\ -4.0}$

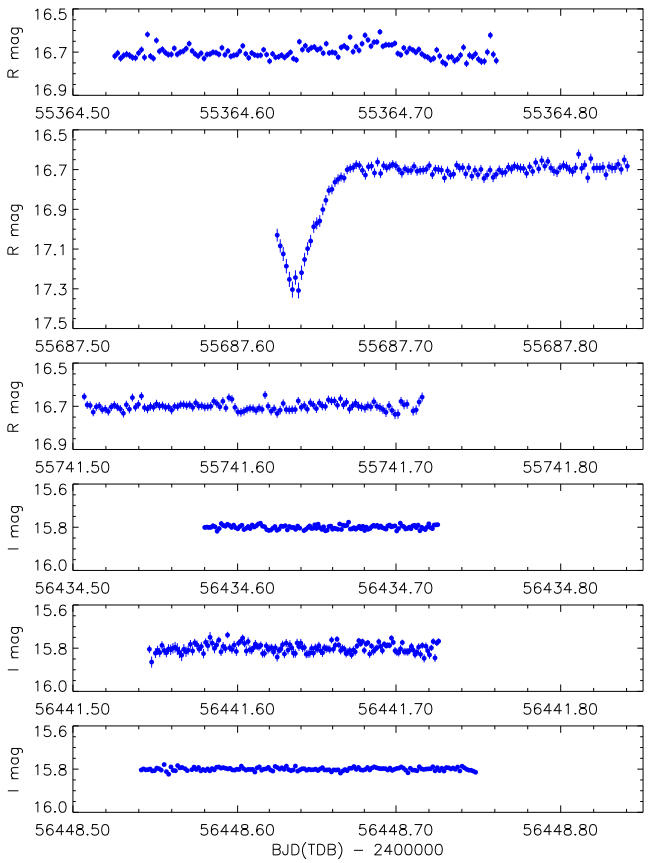

Figure 8. The light curves of the eclipsing binary system near WASP-24 from our observations. Each light curve has been shifted to an out-of-eclipse magnitude of $R = 16.7$ (Zacharias et al. 2004) or $I = 15.8$.

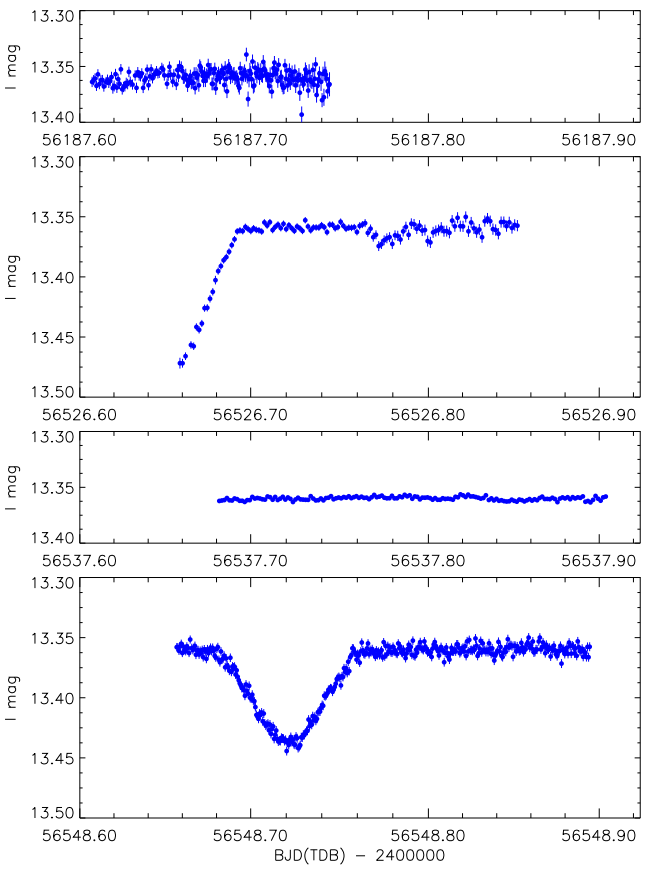

Figure 9. The light curves of the eclipsing binary system near WASP-26 from our observations. Each light curve has been shifted to an out-of-eclipse magnitude of $I = 13.36$, calculated from its spectral type and observed V magnitude.

7 ECLIPSING BINARY STAR SYSTEMS NEAR WASP-24 AND WASP-26

Street et al. (2010) found the closest detected star to WASP-24 (21.2 arcsec) to be a detached eclipsing binary system. It showed eclipses of depth 0.8 mag in four of their follow-up photometric data sets, suggesting an orbital period of 1.156 d. Its faintness ($V = 17.97$) means that it was not measurable in the SuperWASP images. We observed one eclipse, on the night of 2011/05/05 (Fig. 8). This confirms the eclipsing nature of the object, but is not helpful in deducing its orbital period. Further observations of this eclipsing binary would be useful in pinning down the mass–radius relation for low-mass main-sequence stars (e.g. López-Morales 2007; Torres, Andersen & Giménez 2010).

In two of our data sets for WASP-26, we detected eclipses on one object which appears to be a previously unknown detached eclipsing binary system. Its sky position is approximately RA = 00:18:26.5, Dec. = −15:11:49 (J2000). The AAVSO Photometric All-Sky Survey gives apparent magnitudes of $B = 16.02 \pm 0.07$ and $V = 14.98 \pm 0.02$ (Henden et al. 2012). The Two Micron All-Sky Survey lists it under the designation 2MASS J00182645−1511492

(Skrutskie et al. 2006), and its colour of $J - K = 0.72$ implies a spectral type of approximately K4 V (Currie et al. 2010). The object is not listed in the General Catalogue of Variable Stars (GCVS)[10] or the AAVSO Variable Star Index (VSX).[11]

Two eclipses were seen in the 2MASS J00182645−1511492 system, separated by approximately 22.1 d Fig. 9. The first was only partially observed and has a depth of at least 0.11 mag, whereas the full duration of the second eclipse was seen, with a depth of 0.08 mag. The different depths mean that the former is a primary and the latter a secondary eclipse. The orbital period cannot be determined from these data, but is likely quite short as the eclipses do not last long. The SuperWASP survey (Pollacco et al. 2006) has obtained 5800 observations of this object, but these show no obvious variability due to the faintness of the object and the shallowness of the eclipses. Whilst it would be a useful probe of the properties of stars on the lower main sequence, 2MASS J00182645−1511492 is not a particularly promising object for further study due to its shallow eclipses, which makes the measurement of precise photometric parameters difficult, and unknown orbital period.

8 SUMMARY AND CONCLUSIONS

We have presented extensive photometric observations of three Southern hemisphere transiting planetary systems discovered by SuperWASP. All three systems have spectroscopic measurements of the RM effect which are consistent with orbital alignment; two have also been observed with *Spitzer*. Our observations of the third, WASP-25, comprise the first follow-up photometry of this object since its discovery paper.

Our data cover 13 transits of the gas giant planets in front of their host stars, plus single-epoch high-resolution images taken with a Lucky Imaging camera. From these observations, and published spectroscopic measurements, we have measured the orbital ephemerides and physical properties of the systems to high precision. Care was taken to propagate random errors for all quantities and assess separate statistical errors for those quantities whose evaluation depends on the use of theoretical stellar models. Previously published studies of all three objects are in good agreement with our refined values, although we find evidence that their error estimates are unrealistically small.

We have observed one eclipse for the known eclipsing binary very close to WASP-24, and discovered a new K4 V detached eclipsing binary 4.25 arcmin north of WASP-26. We have observed part of one primary eclipse and a full secondary eclipse for the latter object, but are not able to measure its orbital period from these observations.

Fig. 10 shows a plot of planet radius versus mass for all known TEPs (data taken from the TEPCat[12] catalogue on 2014/02/15). WASP-24 b and WASP-26 b are representative of the dominant population of Hot Jupiters, with masses near $1.0M_{\rm Jup}$. WASP-25 b appears near the mid-point of a second cluster of planets with masses of approximately 0.5–$0.7M_{\rm Jup}$; such objects are sometimes termed 'Hot Saturns' although they are more massive than Saturn itself ($0.3M_{\rm Jup}$).

All three planets have radii greater than predicted by theoretical models for gaseous bodies without a heavy-element core (Bodenheimer, Laughlin & Lin 2003; Fortney, Marley & Barnes 2007; Baraffe, Chabrier & Barman 2008) so exhibit the inflated radii commonly observed for Hot Jupiters (e.g. Enoch, Collier Cameron & Horne 2012, and references therein). Its deep transit and low surface gravity make WASP-25 b a good candidate for transmission photometry and spectroscopy to probe the atmospheric properties of a transiting gas giant planet (see Bento et al. 2014).

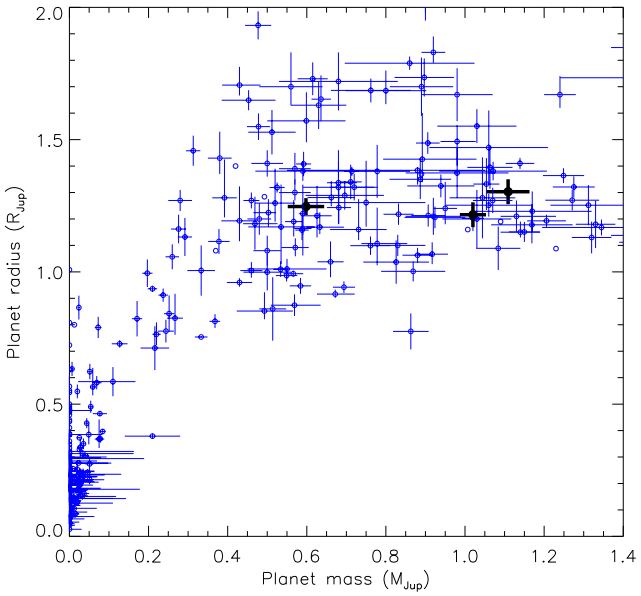

Figure 10. Plot of planet radii versus their masses. WASP-24 b, WASP-25b and WASP-26b are indicated using black filled circles. The overall population of planets is shown using blue open circles, using data taken from TEPCat on 2014/02/15. Error bars are suppressed for clarity if they are larger than $0.2M_{\rm Jup}$ or $0.2R_{\rm Jup}$. The outlier with a mass of $0.86M_{\rm Jup}$ but a radius of only $0.78R_{\rm Jup}$ is the recently discovered system WASP-59 (Hébrard et al. 2013).

ACKNOWLEDGEMENTS

The operation of the Danish 1.54 m telescope is financed by a grant to UGJ from the Danish Natural Science Research Council. The reduced light curves presented in this work will be made available at the CDS (http://vizier.u-strasbg.fr/) and at http://www.astro.keele.ac.uk/∼jkt/. J Southworth acknowledges financial support from STFC in the form of an Advanced Fellowship. The research leading to these results has received funding from the European Community's Seventh Framework Programme (FP7/2007-2013/) under grant agreement nos. 229517 and 268421. Funding for the Stellar Astrophysics Centre (SAC) is provided by The Danish National Research Foundation. This publication was supported by grants NPRP 09-476-1-078 and NPRP X-019-1-006 from Qatar National Research Fund (a member of Qatar Foundation). TCH acknowledges financial support from the Korea Research Council for Fundamental Science and Technology (KRCF) through the Young Research Scientist Fellowship Programme and is supported by the KASI (Korea Astronomy and Space Science Institute) grant 2012-1-410-02/2013-9-400-00. SG, XW and XF acknowledge the support from NSFC under the grant no. 10873031. The research is supported by the ASTERISK project (ASTERoseismic Investigations with SONG and Kepler) funded by the European Research Council (grant agreement no. 267864). DR, YD, AE, FF (ARC), OW (FNRS research fellow) and J Surdej acknowledge support from the Communauté française de Belgique – Actions de recherche concertées – Académie Wallonie-Europe. The following

[10] http://www.sai.msu.su/gcvs/gcvs/
[11] http://www.aavso.org/vsx
[12] The TEPCat is available at `http://www.astro.keele.ac.uk/jkt/tepcat/`.

internet-based resources were used in research for this paper: the ESO Digitized Sky Survey; the NASA Astrophysics Data System; the SIMBAD data base and VizieR catalogue access tool operated at CDS, Strasbourg, France; and the arXiv scientific paper preprint service operated by Cornell University. We thank the anonymous referee for a helpful report.

REFERENCES

Albrecht S. et al., 2012, ApJ, 757, 18
Anderson D. R. et al., 2011, A&A, 534, A16
Baraffe I., Chabrier G., Barman T., 2008, A&A, 482, 315
Bento J. et al., 2014, MNRAS, 437, 1511
Bodenheimer P., Laughlin G., Lin D. N. C., 2003, ApJ, 592, 555
Brown D. J. A. et al., 2012, MNRAS, 423, 1503
Carter J. A., Yee J. C., Eastman J., Gaudi B. S., Winn J. N., 2008, ApJ, 689, 499
Claret A., 2004, A&A, 424, 919
Currie T. et al., 2010, ApJS, 186, 191
Daemgen S., Hormuth F., Brandner W., Bergfors C., Janson M., Hippler S., Henning T., 2009, A&A, 498, 567
Demarque P., Woo J.-H., Kim Y.-C., Yi S. K., 2004, ApJS, 155, 667
Dotter A., Chaboyer B., Jevremović D., Kostov V., Baron E., Ferguson J. W., 2008, ApJS, 178, 89
Eastman J., Siverd R., Gaudi B. S., 2010, PASP, 122, 935
Enoch B., Collier Cameron A., Parley N. R., Hebb L., 2010, A&A, 516, A33
Enoch B. et al., 2011, MNRAS, 410, 1631
Enoch B., Collier Cameron A., Horne K., 2012, A&A, 540, A99
Fortney J. J., Marley M. S., Barnes J. W., 2007, ApJ, 659, 1661
Gibson N. P. et al., 2009, ApJ, 700, 1078
Hébrard G. et al., 2013, A&A, 549, A134
Henden A. A., Levine S. E., Terrell D., Smith T. C., Welch D., 2012, J. Am. Assoc. Var. Star Obs., 40, 430
Knutson H. A. et al., 2014, ApJ, 785, 126
Lillo-Box J., Barrado D., Bouy H., 2014, A&A, 566, A103
López-Morales M., 2007, ApJ, 660, 732
McLaughlin D. B., 1924, ApJ, 60, 22
Mahtani D. P. et al., 2013, MNRAS, 432, 693
Markwardt C. B., 2009, in Bohlender D. A., Durand D., Dowler P., ASP Conf. Ser. Vol. 411 Astronomical Data Analysis Software and Systems XVIII. Astron. Soc. Pac., San Francisco, p. 251
Maxted P. F. L., Koen C., Smalley B., 2011, MNRAS, 418, 1039
Mortier A., Santos N. C., Sousa S. G., Fernandes J. M., Adibekyan V. Z., Delgado Mena E., Montalto M., Israelian G., 2013, A&A, 558, A106
Nelder J. A., Mead R., 1965, Comp. J., 7, 308
Nelson B., Davis W. D., 1972, ApJ, 174, 617
Nikolov N., Chen G., Fortney J., Mancini L., Southworth J., van Boekel R., Henning T., 2013, A&A, 553, A26
Pietrinferni A., Cassisi S., Salaris M., Castelli F., 2004, ApJ, 612, 168
Poddaný S., Brát L., Pejcha O., 2010, New Astron., 15, 297
Pollacco D. L. et al., 2006, PASP, 118, 1407
Popper D. M., Etzel P. B., 1981, AJ, 86, 102
Rossiter R. A., 1924, ApJ, 60, 15
Sada P. V. et al., 2012, PASP, 124, 212
Simpson E. K. et al., 2011, MNRAS, 414, 3023
Skottfelt J. et al., 2013, A&A, 553, A111
Skrutskie M. F. et al., 2006, AJ, 131, 1163
Smalley B. et al., 2010, A&A, 520, A56
Smith A. M. S. et al., 2012, A&A, 545, A93
Southworth J., 2008, MNRAS, 386, 1644
Southworth J., 2009, MNRAS, 394, 272
Southworth J., 2012, MNRAS, 426, 1291
Southworth J., Maxted P. F. L., Smalley B., 2004, MNRAS, 349, 547
Southworth J. et al., 2009a, MNRAS, 396, 1023
Southworth J. et al., 2009b, ApJ, 707, 167
Southworth J. et al., 2010, MNRAS, 408, 1680
Southworth J., Mancini L., Maxted P. F. L., Bruni I., Tregloan-Reed J., Barbieri M., Ruocco N., Wheatley P. J., 2012, MNRAS, 422, 3099
Southworth J. et al., 2013, MNRAS, 434, 1300
Stetson P. B., 1987, PASP, 99, 191
Street R. A. et al., 2010, ApJ, 720, 337
Torres G., Andersen J., Giménez A., 2010, A&AR, 18, 67
Torres G., Fischer D. A., Sozzetti A., Buchhave L. A., Winn J. N., Holman M. J., Carter J. A., 2012, ApJ, 757, 161
VandenBerg D. A., Bergbusch P. A., Dowler P. D., 2006, ApJS, 162, 375
Zacharias N., Monet D. G., Levine S. E., Urban S. E., Gaume R., Wycoff G. L., 2004, Am. Astron. Soc. Meeting Abstr. 36, 1418

SUPPORTING INFORMATION

Additional Supporting Information may be found in the online version of this article:

Appendix.
(http://mnras.oxfordjournals.org/lookup/suppl/doi:10.1093/mnras/stu1492/-/DC1).

Please note: Oxford University Press are not responsible for the content or functionality of any supporting materials supplied by the authors. Any queries (other than missing material) should be directed to the corresponding author for the article.

[1]*Astrophysics Group, Keele University, Staffordshire ST5 5BG, UK*
[2]*Korea Astronomy and Space Science Institute, Daejeon 305-348, Republic of Korea*
[3]*HE Space Operations GmbH, Flughafenallee 24, D-28199 Bremen, Germany*
[4]*Dipartimento di Fisica 'E.R. Caianiello', Università di Salerno, Via Giovanni Paolo II 132, I-84084 Fisciano (SA), Italy*
[5]*Istituto Internazionale per gli Alti Studi Scientifici (IIASS), I-84019 Vietri Sul Mare (SA), Italy*
[6]*SUPA, University of St Andrews, School of Physics and Astronomy, North Haugh, St Andrews KY16 9SS, UK*
[7]*Astronomisches Rechen-Institut, Zentrum für Astronomie, Universität Heidelberg, Mönchhofstraße 12-14, D-69120 Heidelberg, Germany*
[8]*Yunnan Observatories, Chinese Academy of Sciences, Kunming 650011, China*
[9]*Key Laboratory for the Structure and Evolution of Celestial Objects, Chinese Academy of Sciences, Kunming 650011, China*
[10]*Niels Bohr Institute & Centre for Star and Planet Formation, University of Copenhagen, Juliane Maries vej 30, DK-2100 Copenhagen Ø, Denmark*
[11]*Jodrell Bank Centre for Astrophysics, University of Manchester, Oxford Road, Manchester M13 9PL, UK*
[12]*Max Planck Institute for Astronomy, Königstuhl 17, D-69117 Heidelberg, Germany*
[13]*Instituto de Astrofísica, Facultad de Física, Pontificia Universidad Católica de Chile, Av. Vicuña Mackenna 4860, 7820436 Macul, Santiago, Chile*
[14]*Instituto de Astronomía – UNAM, Km 103 Carretera Tijuana Ensenada, 422860 Ensenada (Baja Cfa), Mexico*
[15]*Institut für Astrophysik, Georg-August-Universität Göttingen, Friedrich-Hund-Platz 1, D-37077 Göttingen, Germany*
[16]*NASA Ames Research Center, Moffett Field, CA 94035, USA*
[17]*Institut d'Astrophysique et de Géophysique, Université de Liège, B-4000 Liège, Belgium*
[18]*Qatar Environment and Energy Research Institute, Qatar Foundation, Tornado Tower, Floor 19, PO Box 5825 Doha, Qatar*
[19]*Department of Astronomy, Boston University, 725 Commonwealth Avenue, Boston, MA 02215, USA*
[20]*Istituto Nazionale di Fisica Nucleare, Sezione di Napoli, I-80126 Napoli, Italy*
[21]*Hamburger Sternwarte, Universität Hamburg, Gojenbergsweg 112, D-21029 Hamburg, Germany*

[22]*Dipartimento di Fisica e Astronomia, Università di Bologna, Viale Berti Pichat 6/2, I-40127 Bologna, Italy*
[23]*Main Astronomical Observatory, Academy of Sciences of Ukraine, vul. Akademika Zabolotnoho 27, UA-03680 Kyiv, Ukraine*
[24]*Aryabhatta Research Institute of Observational Sciences (ARIES), Manora Peak, Nainital 263 129, Uttarakhand, India*
[25]*European Southern Observatory, Karl-Schwarzschild-Straße 2, D-85748 Garching bei München, Germany*
[26]*Stellar Astrophysics Centre (SAC), Department of Physics and Astronomy, Aarhus University, Ny Munkegade 120, DK-8000 Aarhus C, Denmark*
[27]*Space Telescope Science Institute, 3700 San Martin Drive, Baltimore, MD 21218, USA*
[28]*Finnish Centre for Astronomy with ESO (FINCA), University of Turku, Väisäläntie 20, FI-21500 Piikkiö, Finland*
[29]*Department of Astronomy, Ohio State University, 140 W. 18th Ave, Columbus, OH 43210, USA*
[30]*Department of Physics, Sharif University of Technology, P. O. Box 11155-9161 Tehran, Iran*
[31]*Max Planck Institute for Solar System Research, Justus-von-Liebig-Weg 3, D-37077 Göttingen, Germany*
[32]*LCOGT, 6740 Cortona Drive, Suite 102, Goleta, CA 93117, USA*
[33]*School of Mathematical Sciences, Queen Mary, University of London, Mile End Road, London E1 4NS, UK*

This paper has been typeset from a TEX/LATEX file prepared by the author.